

# International Conference on Space Optics—ICSO 2018

Chania, Greece

9–12 October 2018

*Edited by Zoran Sodnik, Nikos Karafolas, and Bruno Cugny*



## ***In-flight validation of SPEX airborne spectro-polarimeter onboard NASA's research aircraft ER-2***

*J. Martijn Smit*

*Jeroen H. Rietjens*

*Antonio di Noia*

*Otto Hasekamp*

*et al.*



icso proceedings



## In-flight validation of SPEX airborne spectro-polarimeter onboard NASA's research aircraft ER-2

J. Martijn Smit<sup>\*a</sup>, Jeroen H. H. Rietjens<sup>a</sup>, Antonio di Noia<sup>a</sup>, Otto P. Hasekamp<sup>a</sup>, Wouter Laauwen<sup>a</sup>, Brian Cairns<sup>b</sup>, Bastiaan van Diedenoven<sup>b</sup>, A. Wasilewski<sup>b</sup> S.

<sup>a</sup>SRON Netherlands Institute for Space Research, Sorbonnelaan 2, 3584 CA Utrecht, the Netherlands;

<sup>b</sup> Goddard Institute for Space Studies, 2880 Broadway, New York, NY 10025 USA

### ABSTRACT

High accuracy multi-angle polarimetry is of crucial importance for remote sensing of aerosol and cloud properties with accuracies demanded by climate and air quality studies. In this contribution, we provide a detailed description of the multi-angle spectro-polarimetric instrument "SPEX airborne" that was developed to operate from NASA's high altitude research aircraft ER-2. SPEX airborne delivers measurements of radiance and linear polarization at nine fixed viewports with angles equally distributed over a total angular range of 112°, at visual wavelength in the range 400-760nm. Each viewport acts as a pushbroom spectrometer with a swath of 6°. SPEX airborne participated in the recent the ACEPOL campaign in October-November 2017 when it flew together with NASA's Research Scanning Polarimeter (RSP), the Airborne Multiangle SpectroPolarimetric Imager (AirMSPI), and the Airborne Hyper-Angular Rainbow Polarimeter (AirHARP). We compare polarimetric and radiometric measurements from SPEX airborne with those collected by RSP at four visible wavelength bands. Simultaneous measurements were made while flying over widely different scenes, under different illumination and meteorological conditions. This provided a large dynamic range in radiometric and polarimetric values. We find that the Degree of Linear Polarization (DoLP) measured by both instruments agrees well with a RMS differences of ~0.005 as the best result for 555nm. For radiance measurements excellent agreement is obtained with a RMS difference of ~4%. The in-flight comparison results provide verification of SPEX airborne's capability to deliver high-quality data.

**Keywords:** spectro-polarimetry, multi-angle, airborne, remote sensing, aerosols

### 1. INTRODUCTION

It is a well-established fact that aerosol impact our climate and air-quality significantly. The present situation is that the overall cooling effect due to aerosol may be as large as the heating effect of the strongest greenhouse gas. However, large uncertainties in aerosol-cloud interactions hamper reliable climate forecasts. These uncertainties must urgently be reduced, by improving observations of aerosol on a global scale, and by extending the parameter space of measured particle properties. Aerosol (and cloud) properties can only be unambiguously determined from space-based instruments that measure both intensity and polarization at multiple viewing angles and multiple wavelength with a wide swath to enable global coverage at daily timescales [1]-[5]. So far, the only polarimeters in Earth-orbit have been the series of French POLDER (1-2-3) instruments from CNES. POLDER-3 flew on the French PARASOL satellite from 2004 to 2013 [6]. POLDER will reincarnate as 3MI to fly on a series of satellites as part of the Metop-SG programme. In the past two decades, several next-generation polarimeters been developed: RSP [7][8], AirMSPI [12][13][14], and PACS/AirHARP [15]. AirMSPI and AirHARP will be deployed in space in the near future as MAIA and HARP [16] respectively. These instruments use different measurement techniques and have been developed with different design drivers such as ground coverage (swath), spatial resolution, spectral sampling, and polarimetric performance. In the Netherlands, SRON has engaged on realization of a space-based spectro-polarimeter together with several Dutch partner institutes. The original Optical Module of SPEX airborne was designed and built by a consortium of Dutch knowledge institutes and space technology companies [17][18]. Preliminary characterization & performance tests under laboratory conditions demonstrated excellent performance [19]-[23], indicating that the instrument concept would be capable to meet stringent performance requirements for aerosol characterization of the Earth's atmosphere. SPEX airborne was subsequently

\* [j.m.smit@sron.nl](mailto:j.m.smit@sron.nl), phone +31 88 777 5680 ; fax +31 88 777 5601,

developed by SRON as a payload for NASA's high altitude atmospheric research aircraft ER-2. The realization of SPEX airborne is part of a development in The Netherlands towards several possible realizations of space-based, SPEX-like instruments [24]. The first space-borne version is SPEXone, a compact, 6 dm<sup>3</sup>-sized spectropolarimeter with five fixed viewing angles is being developed for NASA's Phytoplankton, Aerosols, Clouds and ocean Ecosystems (PACE) mission, scheduled for launch in 2022. Details of SPEXone, including optical and mechanical design, integration, test & verification approach, and overall development status, are provided in these proceedings [25].

## 2. SPEX AIRBORNE INSTRUMENT

SPEX (Spectro-polarimeter for Planetary Exploration) airborne employs the spectral modulation technique [26] to accurately measure the degree of linear polarization (DoLP) and angle of linear polarization (AoLP) in the spectral range 400-760 nm with a spectral resolution of 7-20 nm. The spectral intensity (radiance) is being measured at higher spectral resolution of 3 nm. SPEX airborne performs multi-angle measurements at 9 fixed viewing angles ranging between  $\pm 56^\circ$  degrees. At each viewing angle, the instrument has an instantaneous field of view (IFOV) of  $6^\circ$  (swath) x  $1.0^\circ$  (along-track), with an effective ground pixel angular size of  $0.2^\circ$  (swath) x  $1.0^\circ$  (along track). SPEX airborne uses a single CCD detector to record modulated spectra from all nine viewing angles simultaneously at a sample rate of 1.75 seconds per CCD image. The airborne configuration as flown on NASA's atmospheric research aircraft ER-2 is rendered in Figure 1. The system includes a Structural Support Unit (SSU), onto which are mounted an Instrument Power Unit (IPU), an Instrument Control Unit (ICU), and an alignment unit (AU). The AU holds, enclosed inside a thermal shield, the Optical Module (OM), a CCD camera and a reference measurement unit (RMU). The payload is mounted inside the rear section of a unpressurized pod attached to the wings on the ER-2 aircraft, where it has a clear view downwards over the full angular range. The instrument is exposed directly to the exterior environment – an intervening window would alter the state of polarization of incident light in an uncontrolled manner. Instrument specifications are provided in Table 1. In this table, the quoted uncertainty for the DoLP that can be obtained in-flight is a target value. Verification of this target is reported in Section 6.3.

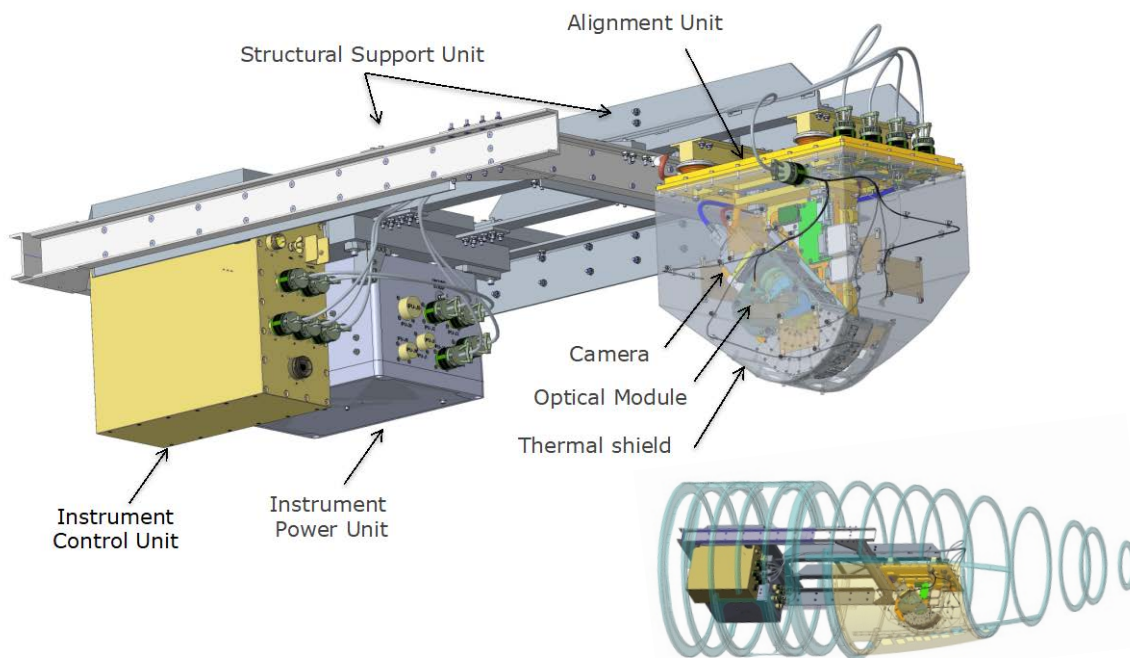


Figure 1. SPEX airborne payload for the ER-2 aircraft

Table 1: SPEX airborne specifications

Spectral range	400-760 nm
Spectral resolution DoLP	7-30 nm
Spectral resolution radiance	3 nm
Uncertainty DoLP	Lab: 0.002 Flight: 0.005
Uncertainty radiance	4% <sup>(a)</sup>
Viewing directions	0°, ±14°, ±28°, ±42°, ±56°
Swath Field of view	6° 2.5 km <sup>(b)</sup>
FOV resolution	0.2°x 1° 60 x 350 m <sup>2</sup> <sup>(b)</sup>
Mass	75 kg IPU: 9 kg, ICU: 12 kg AU: 10kg, OM: 1kg SSU: 33kg
Input power	28 Volt DC / 24 Amp max
Power consumption	75 Watt max IPU: 15 W, ICU: 40 W Camera+RMU: 9W
Dimensions	1320 x 470 x 718 mm <sup>3</sup>

<sup>(a)</sup> Estimated accuracy of reference spectrometer used for radiometric calibration; <sup>(b)</sup> At 20 km altitude, nadir viewport.

## 2.1 Optical Module

The Optical Module consists of nine identical pre-slit optical units –the polarization encoders– and a spectrometer. The interface between the two is an array of slits. The optical system, including several light paths in the plane of spectral dispersion, are shown in Figure 2. A physical representation of the module plus camera, mounted on a baseplate, is shown in Figure 4. Nine identical units with pre-slit polarization modulation optics (PMO) are responsible for encoding the linear degree of polarization of the incoming light. Light passes the polarization encoder optics first, ensuring that no instrument polarization corrupts the signal before polarimetric encoding occurs. Two spectrally modulated beams exiting each of the nine polarization encoders are focused in pairs, by a 4.4 mm diameter lenslet with a focal length of 10 mm, via a folding mirror onto a pair of slits of an array of eighteen identical slits. Each slit measures 0.2x1.4 mm<sup>2</sup>. In the spectrometer, light is collimated via a spherical mirror, then folded via a flat mirror, and spectrally dispersed by a holographic grating. Light is subsequently re-focused by a set of a-spherical lenses onto a single CCD detector. The effective wavelength range of 400-760 is determined by the transmissive optics becoming opaque below 400nm, and by high order overlap from the grating at wavelengths above 760nm.

Encoding of the state of linear polarization by the PMO occurs by a combination of three optical elements: a quarter wave retarder, a (composite) multiple order retarder, and a polarizing beam-splitter [14], as shown schematically in Figure 3. Light passing through the MOR undergoes a wavelength-dependent phase shift, resulting in a change of incident linearly polarized light along the vertical into circular, elliptical or linear, as a function of wavelength. The PBS acts as a linear polarizer; the projection of the state of polarization onto the polarizer axis determines the intensity of the light passing through. The net effect is a sinusoidal modulation of the intensity spectrum:

$$I_{\pm}(\lambda) = \frac{1}{2} I(\lambda) \left\{ 1 \pm \text{DoLP} \cos \left( \frac{2\pi\delta}{\lambda} + 2 \text{AoLP} \right) \right\},$$

(Error!  
Bookmark

not  
defined.1)

where  $I(\lambda)$  is the incident spectral radiance,  $\lambda$  is wavelength,  $\delta$  is the retardance of the MOR,  $I_+(\lambda)$  and  $I(\lambda)$  are the two beams exiting the PMO. The retardance  $\delta$  is  $\sim 21\mu\text{m}$ , resulting in a gradually increasing modulation period from 7nm at 400nm up to 28nm at 760nm. The modulation amplitude scales with the degree of linear polarization (DoLP), and the phase is equal to angle of linear polarization (AoLP). Two beams  $I_+(\lambda)$  and  $I(\lambda)$  have orthogonal polarization, whereby the modulations are precisely in anti-phase. The function of the QWR is to change linearly polarized light with polarization axis along the optical axes of the MOR into circularly polarized light.

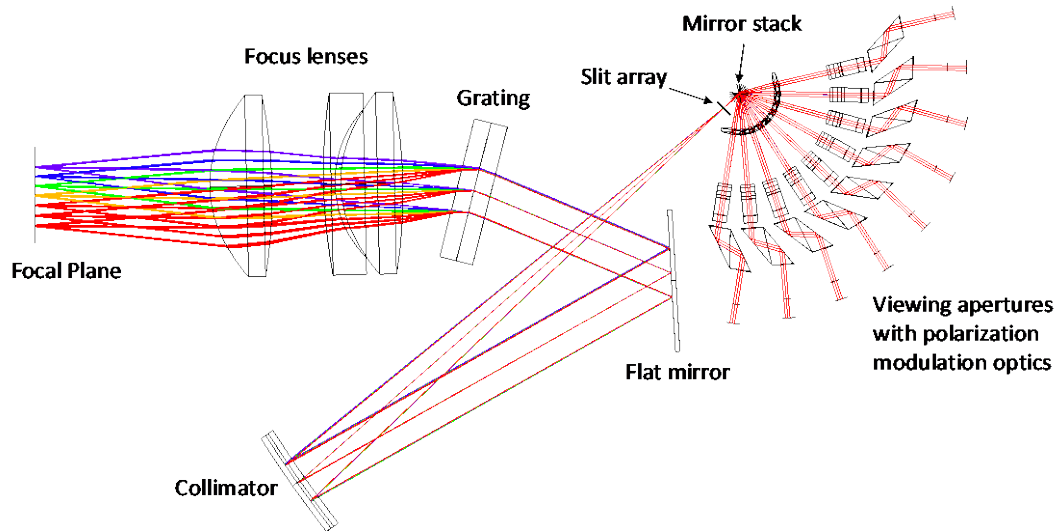


Figure 2. Representation of the OM optical components and light paths entering via the polarization modulation optics. The slit array is oriented normal to the paper.

From Eq.(1) it is readily seen that the sum of the two modulation spectra  $I_+(\lambda)$  and  $I(\lambda)$  is modulation free and provides a direct determination of the spectral radiation field  $I(\lambda)$ . DoLP and AoLP are derived by fitting the scaled modulation spectrum

$$M(\lambda) = \frac{I_+(\lambda) - I(\lambda)}{I_+(\lambda) + I(\lambda)}$$

(Error!  
Bookmark  
not  
defined.2)

with a fit function

$$M_{\text{fit}}(\lambda) = W(\lambda) \text{DoLP} \cos\left(\frac{2\pi\delta}{\lambda} + 2 \text{AoLP}\right)$$

(Error!  
Bookmark  
not  
defined.3)

over wavelength intervals one modulation period long. Equation (3) includes the polarimetric efficiency  $W(\lambda)$  to account for spectral smearing of the modulations by the slit and defocus. Note that in the ratio Eq.(2), the radiation field  $I(\lambda)$  cancels and that the polarimetric efficiency  $W$  and the retardance  $\delta$  are the only instrumental parameters in Eqs.(1-2). Their (wavelength dependent) values are determined from polarization calibration measurements. One of the advantages of the spectral modulation method is that it provides a “snapshot” measurement of the spectral radiance and polarization with a single measurement. This feature is essential in obtaining high-accuracy polarization performance.

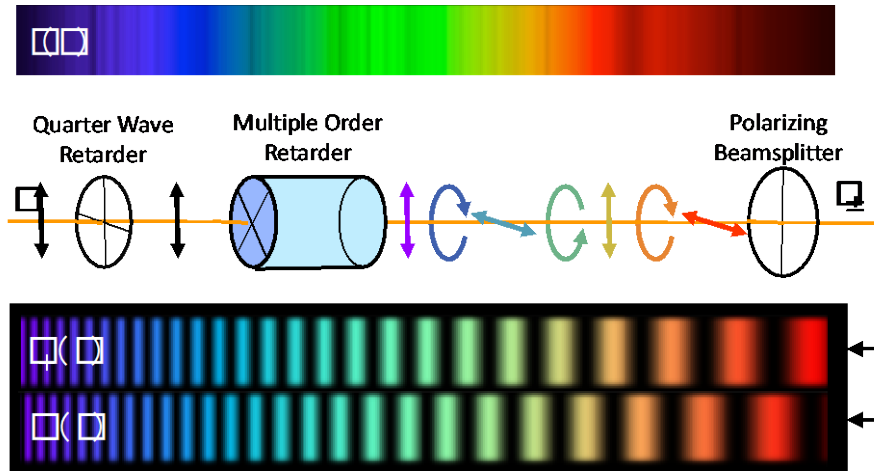


Figure 3. Schematic representation spectral modulation via the polarization modulation optics.

The instantaneous field of view in the along-track direction is determined by the slit width and the focal length of the small lenslet, and is  $1^\circ$ . In the cross-track direction, the slit provides a  $7^\circ$  field of view of which the central  $6^\circ$  is collected to avoid vignetting at the edges. In the focal plane the spatial resolution is  $0.1^\circ$  per pixel. We typically combine two spatial pixels so that the effective cross-track field of view is  $0.2^\circ$ . The effective ground pixel size is determined by the 1.75 sec integration time per image (see next section), the cruise altitude of the aircraft at 20km and the ground speed of 210m/s. The effective ground pixel measures  $70 \times 350 \text{ m}^2$  for the nadir viewport, and increases with viewing angle, up to  $125 \times 1120 \text{ m}^2$  for the aft- and foremost viewing angles at  $\pm 56^\circ$ . The spectrometer optics are contained in a stiff monolithic aluminum structure, with the PMO contained in separate housings. An external baffle, part of the Optical Module housing (see Figure 4), blocks light from outside the nominal field of view. The OMA is mounted onto a baseplate that also holds the camera, the RMU, and the optical reference cube. The camera is mounted via an interface bracket that allows for alignment of the CCD sensor relative with the focal plane (Section 2.3).

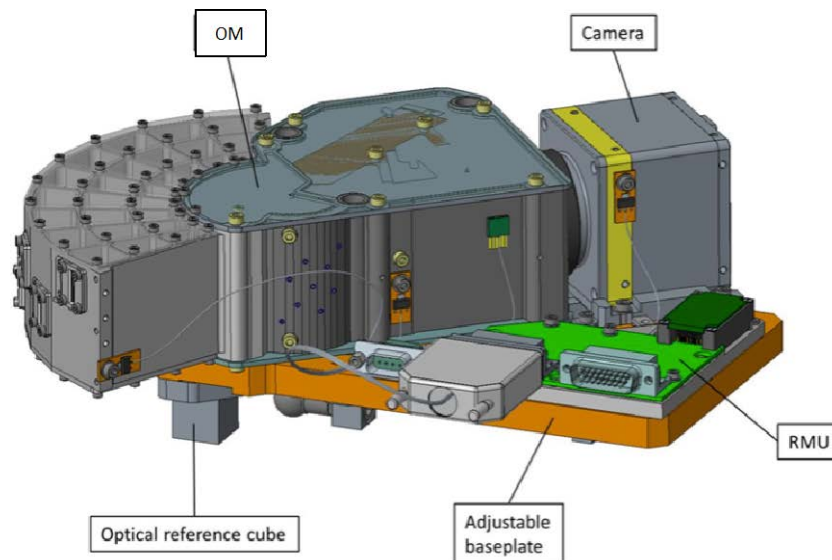


Figure 4. Optical Module mounted on the adjustable baseplate, together with Bobcat CCD camera, the reference measurement unit (RMU), and reference cube.

The camera is a 12 bit BOBCAT B2041M(onochrome), with a KAI-04070 interline transfer CCD from ON Semiconductor. The CCD has  $2072 \times 2072$  pixels of  $7.4 \mu\text{m}$ , with a full well of  $40.000e^-$ , readout noise of  $12e^-$  rms



Module on its baseplate (including camera, RMU and reference cube) and re-mounting without loss of alignment. Being able to remove the OM is beneficial for the purpose of instrument calibration, which requires only the Optical Module. Using the AU, possible misalignment with the aircraft reference can in principle be adjusted. In particular, compensation of a yaw-angle mismatch would be desirable to optimize projected swath overlap of fore and aft viewports. During the ACEPOL campaign, the only angular adjustments made was a fixed roll-offset of  $0.8^\circ$  to match the average orientation of the wing relative to the fuselage during the flight. With the plane fueled up, the wings flex “up” a bit, and relax during the flight as fuel is consumed. With the invoked offset, the center viewport is pointing close to nadir half-way during the flight, and also effects optimized viewing angle overlap of SPEX airborne and RSP (inside the opposite wing-pod).

### 3. DATA PROCESSING

Post-flight, raw images (Level 0) are converted into time-ordered calibrated measurements of radiance, DoLP and AoLP (Level 1B), and subsequently collected on a common spatial grid (Level 1C). Data processing include dark image correction, spectral extraction, wavelength annotation, radiometric correction, and extraction of the state of polarization. After dark image correction, spectra are extracted pair-wise from the raw images, where each spectrum of a pair belongs to the same viewport-swath angle element, with spectral modulations in anti-phase. The spectra are annotated with wavelengths determined from wavelength calibration measurements, and interpolated on a common wavelength grid. To account for differences in transmission and efficiency for the two beams through the spectrometer, separate radiometric calibration factors are applied to the two spectra. Subsequently, the sum-spectrum is modulation free, providing radiance in units  $\text{Watt/m}^2/\text{nm}/\text{steradian}$ . From the scaled difference (see Eq.(2)), containing only the modulations, DoLP and AoLP are derived by fitting the modulation pattern with a sinusoidal function. This process is denoted as “demodulation” and is described in more detail in [22] and [32]. Hereafter, the data are assigned a geographical longitude and latitude by means of a so-called “direct georeferencing” algorithm. The intersection is determined of the viewing direction of each viewport-swath angle element with the Earth surface, using GPS location data, aircraft roll, pitch and heading information, a model of the flexing of the wing, and a 250m resolution SRTM Digital Elevation Model [31]. In addition, the orientation of the instrument relative to the aircraft reference frame is included that is obtained from comparisons of georeferenced SPEX imagery with high resolution reference imagery (Section 6.1). In the final step, geolocated radiances, DoLPs and AoLPs are interpolated on a common spatial grid. Each grid point is annotated with its latitude, longitude, and altitude, and, for each datum, with viewing zenith and azimuth angles. The grid step size (in meters) can be defined by the user, where typically we use  $1000 \times 1000 \text{m}^2$ .

### 4. INSTRUMENT CALIBRATION

Calibration of SPEX airborne include standard calibration operations used for pushbroom spectrometers, including wavelength calibration, radiometric calibration and geometrical calibration. In all calibration measurements, the OMA (plus camera, on the baseplate) was unmounted from the airborne configuration and installed on a dedicated rotation-translation mount. The mount includes an interface plate such that the OMA can be rotated around an axis that coincides exactly with vertex of light beams of the viewports in Figure 2. This way, the PMO of each viewports is positioned at the same location in the test setup. Wavelength calibration measurements were performed in-house using an HG-1 spectral line source Ocean Optics in a two-lens setup to illuminate the  $7^\circ$  swath in one go. Wavelength calibration is performed with an accuracy of 0.2 nm. Geometrical calibration provides the line of sight of each pixel relative to the reference cube. Calibration measurements included a white light point source in combination with a laser, both placed on a vertical stage with large range to scan the swath. A theodolite was used to determine the direction of the laser relative to the reference cube on the baseplate, thereby tying also the white light point source to the instrument frame. SPEX airborne was calibrated radiometrically and polarimetrically at JPL facilities with equipment established for calibration and validation of the Airborne Multiangle SpectroPolarimetric Imager (AirMSPI) [14]. Radiometric calibration measurements were made using a large integrating sphere, with reference spectra obtained with a hand-held FieldSpec spectrometer. The spectrometer is calibrated regularly against a NIST traceable light source and provides 4% accuracy over the full wavelength range 350-2500nm. For polarimetric calibration we used the Polarization Stage Generator-2 (PSG-2), which holds a (smaller) integrating sphere in combination with a set of polarizing elements that can be inserted in the light beam and rotated around the optical beam axis. For polarimetric calibration a wiregrid linear polarizer is inserted to generate a 100% polarized beam. A set of tilted glass plates, each with a different tilt angle, can be inserted to provide

partial polarized light. Such measurements are used to verify polarimetric calibration of the instrument. Using the PSG-2, the uncertainty of the SPEX airborne DoLP is found to be in the range 0.002-0.004 [32].

## 5. RESEARCH SCANNING POLARIMETER

The Research Scanning Polarimeter [7], operated by NASA-GISS, is an airborne polarimeter instrument of the same type as the Aerosol Polarimetry Sensor payload of the Glory mission [9] that was lost after a failed launch in 2011. RSP measures radiance and linear polarization state over a viewing angular range of  $\pm 60^\circ$  around the instrument downward pointing normal. A scanning mirror assembly uses matched mirrors illuminated at  $45^\circ$ , with reflection planes at  $90^\circ$  to one another, such that the state of polarization of incident radiation is preserved. One complete scan is made every 0.84s, providing data at 152 sectors of the scan angular range ( $0.8^\circ$  resolution). Light reflected off the mirror systems enters a collection of six telescopes, with coinciding 14mrad fields of view. The state of linear polarization is determined per telescope pair, where behind each telescope light passes a polarization beamsplitter. Beamsplitters are oriented such that light is projected along four linear polarization directions, oriented for one beamsplitter at  $0^\circ$  and  $90^\circ$  relative to the scanning plane, and the other at  $45^\circ$  and  $135^\circ$ . This way, incident radiation is decomposed along four linear polarization directions, from which three Stokes parameters  $I$  (radiance),  $Q$  and  $V$  (linear polarization components) are reconstructed. For each telescope pair, light is sampled over three wavelength bands using dichroic mirrors, providing measurements at nine wavelength bands: 410(30), 470(20), 555(20), 670(20), 864(20), 960(20), 1593(60), 1880(90), and 2263(120) nm, where the spectral width of each band is indicated with brackets. Two versions of RSP built in 1999 and 2001, that can be deployed on multiple aircraft. RSP has a long-standing track record of flights. Reported accuracies for DoLP and radiance are 0.002 and 5% respectively [7].



Figure 6. Research Scanning Polarimeter

## 6. AIRBORNE CAMPAIGN

SPEX airborne was deployed on the ER-2 in 2017 to participate in the “Aerosol Characterization from Polarimeters and Lidar (ACEPOL) campaign, together with a suite of polarimeters including RSP, AirMSPI and AirHARP. Two lidars complemented the instrument suite: the High Spectral Resolution Lidar 2 [29] from NASA-Langley, and the Cloud Physics Lidar from NASA-GSFC [30]. The main objective of the ACEPOL campaign is to compare the capabilities of the different polarimeters for retrieval of aerosol microphysical and optical parameters, and to investigate aerosol retrievals using combined polarimeter and lidar data. The campaign was performed during October – November 2017, and included a total of nine flights, targeting predominantly southern California – See Figure 7. Flights were performed on clear sky and cloudy days, over ocean, flat terrain, towns, desert area, mountains, etc. On two flights, small scale forest fires were targeted.

Clear sky flights included passes over AERONET stations. Aerosol loading was low throughout the campaign period, with the Aerosol Optical Thickness below 0.2. Each flight consists of a series of straight ground tracks centered on predefined targets. Tracks are at least 60km in length as required by all the multi-angular polarimeters in order to obtain co-registered views of ground scenes over the full angular scale. At 20km altitude, the atmospheric conditions are benign, allowing the ER-2 to fly steadily with minimal manoeuvring (roll, pitch, & yaw variations less than  $\pm 0.2^\circ$  during a track), resulting in almost perfectly straight ground tracks and optimized overlap between ground-projected fore- and aft viewing directions.

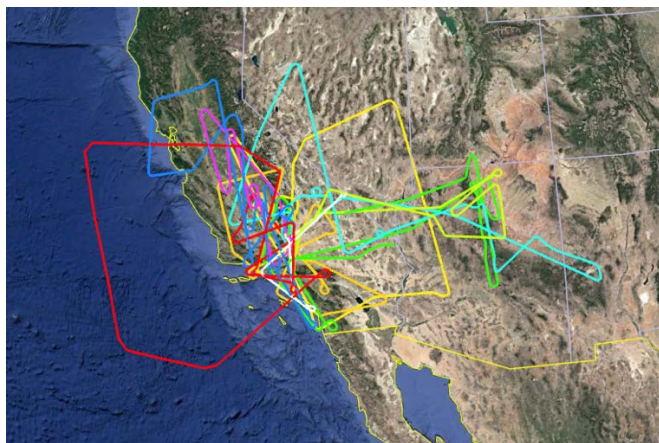


Figure 7. Overview of ACEPOL flights over the USA. Each flight is marked with a different color.

### 6.1 Georeferenced SPEX airborne imagery

Clear sky conditions allow for validation of the geo-located data recorded with SPEX airborne by comparison with reference images. When the geolocation is properly performed, georeferenced imagery from SPEX airborne, represented on a longitude-latitude grid, should coincide with the reference images. Figure 9 shows an example from a segment of a flight on October 23, when the ER-2 passed over the San Francisco Bay. Two panels in the figure display radiance and polarization respectively, both rendered as RGB images, obtained by convolving spectral data with typical RGB response curves. Data are from the nadir viewport which has a projected swath of 2.5km. The reference image is taken from World Imagery service from ArcGIS. Clearly there is good overlap between SPEX airborne and the reference where in particular the coastline in the SPEX airborne imagery lines up well with the reference. The DoLP image provides a complementary view, with high contrast between ocean and land. During this particular segment of the flight, the ER-2 aircraft performed corrective manoeuvring, which shows up as wiggles in the projected data. While such angular motions are not favored for co-registration of multi-angle data because they result in reduced overlap between different viewing angles, they do provide a consistency check of the projection algorithms for large attitude variations of the aircraft. From comparisons between SPEX airborne imagery and World Imagery, performed for multiple tracks from multiple flights, we were able to determine the orientation of the SPEX airborne instrument relative to the ER-2, or, to be more specific, relative the ER-2 navigation data system reference. Along three axes defining ER-2 roll, pitch and yaw angular motions, we find offsets of  $0 \pm 0.2$ ,  $+0.8 \pm 0.5$  and  $0^\circ \pm 0.2$  degrees respectively. The stated accuracies correspond with the IFOV pixel size. Due to the elongated pixel shape, SPEX airborne provides more detail along the swath direction than along track. A pitch offset causes shifts of the images in the along-track direction, while roll and yaw result in shifts along the swath. Therefore roll and yaw offsets are determined somewhat better than the pitch. Only flat terrain was used to determine the instrument alignment, using coastlines and large agriculture fields as matching features. On flat terrain, the effect of illumination in different viewing angles (e.g. shadows, hidden features for outermost viewing angles), which can be misinterpreted as spatial misalignments, is reduced. Color rendering has proven valuable for understanding SPEX airborne imagery and for matching features with those in reference images.

Another example of SPEX airborne imagery is shown in Figure 9, collected on October 27 2018 when a small controlled forest fire occurred in the Grand Canyon. The left panel shows a MODIS image of that day, overlaid with a color image from the AirHARP instrument, and with SPEX airborne placed on top. Both instruments capture the smoke plume and allow to pinpoint the fire which is directly below the brightest spot. Images of the two airborne instruments line up with MODIS and with respect to each other. Because the terrain is erratic, with large variations in height, comparisons like this

provide a strong test for the quality with which the geolocation is performed. Note also that the smoke patterns, a transient feature in time, overlap from both polarimeter instruments. Even though the swath and spatial resolution of SPEX airborne are moderate compared to AirHARP, there is ample detail, giving the impression that SPEX airborne is rendered semi-transparently. In the DoLP image (right panel in Figure 4), the smoke appears dark-brownish; multiple scattering in the smoke depolarizes the light. Again, color rendering of DoLP provides complementary qualitative information. The brownish color of the smoke in the DoLP color image is distinctly different from clouds, which appear as dark shades of gray-blue.

So far, the comparative analysis of SPEX airborne has been made by visual inspection. In the future it is planned to employ more advanced photogrammetry tools for automated image registration and image alignment.



Figure 8. Segment of a flight track over San Francisco Bay. The area shown is 60km x 30km. SPEX airborne data from the nadir viewport is the narrow strip (2.5km wide swath), plotted over a reference image from World Imagery from ArcGIS, ESRI. Left image displays RGB radiance, right panel shows RGB polarization (DoLP).



Figure 9. Flight track over Grand Canyon, capturing a smoke plume from a forest fire. The area shown is 80km x 80km. Left image displays RGB radiance, right panel shows RGB polarization (DoLP). The left image includes a pushbroom-color image from AirHARP, with the SPEX airborne strip overlaid. The background image from MODIS of the same day.

## 6.2 Data comparison methodology

For an inter-comparison of measurements, we must collect data which are coincident in the temporal, spatial and spectral domains, and take into account operational and conceptual differences between the two instruments. SPEX airborne can be considered as a set of nine separate pushbroom imaging spectrometers, each with a swath of  $6^\circ$  and an instantaneous field of view of  $1^\circ \times 0.2^\circ$ . RSP is a scanner, collecting light from within a single  $0.8^\circ$  field of view which repeatedly sweeps along the flight direction (rotating around the pitch axis). On the ER-2, RSP has a useful angular range from  $-63.2^\circ$  to  $+42.7^\circ$ . With each scan, RSP intercepts eight out of nine of SPEX airborne's viewports somewhere along the swath. RSP has overlapping wavelengths with SPEX airborne at 410, 460, 555, and 670 nm. Of these, the 410nm band partly lies outside of SPEX airborne's effective wavelength range. When comparing instrument, RSP is adopted as the reference for

SPEX airborne. With RSP being equipped with in-flight calibration, and having a track record of close to two decades of collecting aerosol and cloud data, its measurements are considered to be among the best to-date.

For an inter-comparison of measurements, we must collect data which are coincident in the temporal, spatial and spectral domains. A straightforward approach would be to collect measurements with coinciding geolocation, with matching longitude and latitude coordinates and matching viewing zenith- and azimuth angles, to within pre-set matching accuracy. For this to work however, pointing knowledge (directly impacting geolocation) must be right on the mark and that cannot be assumed to be the case. For SPEX airborne, knowledge of instrument to aircraft instrument orientation is obtained using rather rudimentary methods which are still in development. A complicating factor is that during the campaign, SPEX airborne was in the right wing-pod, while RSP was in the left. As a consequence the two instruments experienced opposite wing-flex. Level 1 data of the two instruments are obtained with slightly different models of wing-flex. Moreover, the wingflex models describe the average flex of the wings with time and deviations, order of  $0.2^\circ$  inferred from the tilt sensor, occur from track to track. The magnitude of the amount of wingflex may not even be the same for the two wings. Such considerations led to an approach for which as little assumptions are made as possible about the pointing of SPEX airborne: SPEX airborne data are correlated with RSP data in the time domain and best matches are selected. This was done taking several steps. First, RSP data were resampled at the temporal grid of SPEX. Next, SPEX airborne polarization and radiance spectra were folded with the spectral response curves of the four RSP bands to obtain spectrally averaged data at RSP wavelengths (for the 410nm wavelength band, the response curve was cut off at 400nm). Then, the root mean square (rms) difference between SPEX airborne and RSP data was determined per track, for each of SPEX airborne's viewport-swath combination with each of RSP's scan angles. At a given wavelength and viewing angle of SPEX airborne, this results in a two-by-two array of rms values, from which the optimum provides the best-matching RSP scan angle and best-matching angle along the swath of SPEX-airborne. The average of the best-matching RSP scan-angles over all tracks (of all flights) is then determined for each viewport of SPEX airborne. In the final step, the data sampling is repeated for all tracks, but using RSP scan-angles fixed at the average best-matching values, and optimizing only for the swath angle. In this last step a filter is included: the best matching SPEX airborne data should have a swath angle within half a degree from the value predicted by the wingflex model, otherwise it is discarded.

### 6.3 SPEX airborne – RSP comparison results

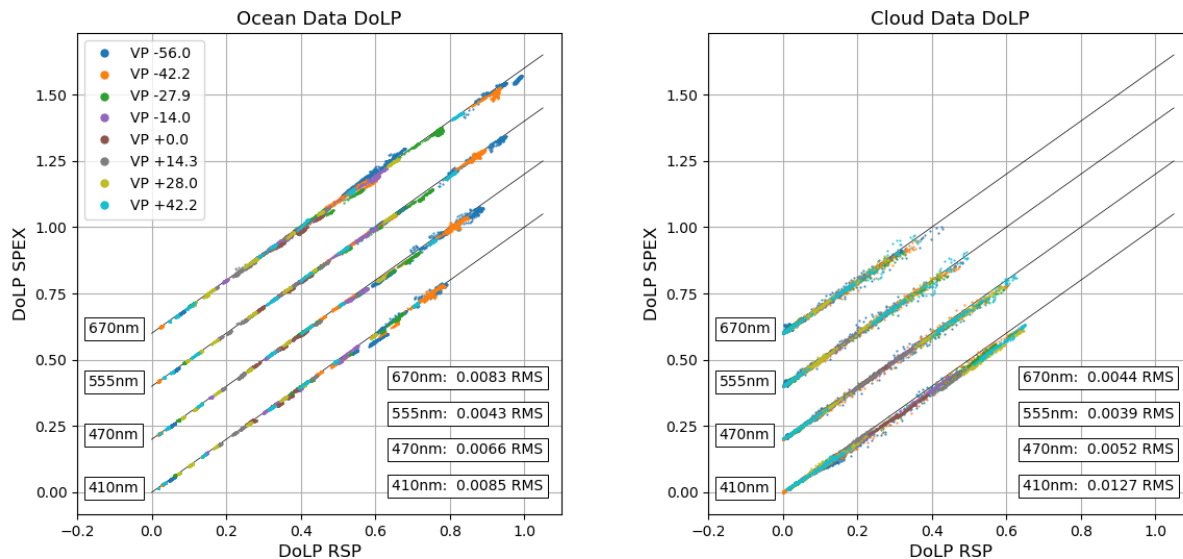
Here we discuss comparisons of polarimetric and radiometric measurements that were made for two types of scenes denoted as “ocean” and “cloud”. The “ocean” scenes include flight tracks over ocean and lakes under clear sky conditions, while “cloud” scenes denote low clouds over land and ocean (not cirrus). These scenes were selected to maximize the dynamic range of polarization and radiance. Ocean data include flights on two days with the ER-2 heading aligned with the principle plane, and the solar zenith angle near the Brewster angle, resulting in DoLP near unity for solar glint observations. An advantage of ocean scenes is that they are very homogeneous, having little variation of intensity and DoLP along the swath. Therefore errors due to pointing mismatches which are amplified by scene inhomogeneities, are reduced. Observations of (thick) clouds provide peak radiance levels at all wavelengths, and minimal DoLP for backscatter viewing geometries. Selected ocean and cloud scenes both comprise eight tracks from four flights. For these selected scenes, the inter-comparison of SPEX airborne with RSP is shown in Figure 10, where the DoLP of SPEX airborne ( $\text{DoLP}_{\text{SPEX}}$ ) is plotted versus RSP ( $\text{DoLP}_{\text{RSP}}$ ) in the upper two panels for ocean and cloud scenes, and the respective radiances,  $I_{\text{SPEX}}$  and  $I_{\text{RSP}}$  are in the lower two panels. Data from different wavelengths are offset successively by fixed amounts along the vertical axis. In each panel the level of agreement between the data is denoted by the root-mean-square values listed per wavelength band. For polarization data, this is the root-mean-square (rms) of all  $\text{DoLP}_{\text{SPEX}} - \text{DoLP}_{\text{RSP}}$  values, while for radiance it the rms is determined of the relative difference  $(\text{DoLP}_{\text{SPEX}} / \text{DoLP}_{\text{RSP}} - 1)$  in percent. Data from different SPEX viewing angles are color coded according to the legend in the top left panel. Almost the complete dynamic range of DoLP, zero to unity, is captured in the dataset. Ocean data almost cover the entire dynamic range of DoLP, with the highest DoLP values obtained over the ocean in sun-glint near the Brewster angle, recorded with SPEX with the aft-most viewing angle at  $-56^\circ$ . For 670nm, DoLP is nearly unity. At shorter wavelengths, the maximum DoLP at the Brewster angle is reduced by atmospheric scattering. Radiance is large in the glint at all wavelengths, but well below the radiances encountered in cloud scenes. In the glint, radiance can potentially saturate the instrument, but due to omnipresent winds during the campaign, the ocean surface was roughened, resulting in reduced reflectance. Lowest DoLP values were recorded over clouds, with values near 0.001, the detection threshold of SPEX airborne.

The level of agreement that we find between SPEX airborne and RSP DoLP measurements varies with wavelength. The best match is found for the 555nm band, which for both scenes is better than the DoLP uncertainty target adopted for SPEX

airborne (0.005). For the ocean scenes, the agreement at 470nm is near the target, while 410nm and 670nm are somewhat out of range. For cloud scenes, agreement is excellent for at all wavelengths except 470nm. At all wavelengths, SPEX airborne DoLP measurements are systematically below RSP by what seems to be a wavelength dependent factor. This is evident most clearly in the 410nm and 470nm cloud measurements, where the slope in the data is below the solid line denoting the  $DoLP_{SPEX} = DoLP_{RSP}$  line. If this slope, which is  $\sim 0.96$  for 410nm, for would be extended to  $DoLP=1$ , then SPEX airborne would end up 0.04 below RSP. In this case the deviation of the slope from unity is the prime cause for the relatively high rms difference. If points would be equally distributed along the slope over the recorded DoLP range 0-0.6, then the rms would be 0.05, accounting for most of the observed 0.085 rms difference. The other part is due to scatter, constituting point-to-point scatter and track-to-track variations. Track to track variation can be inferred from the ocean data (top left panel) where data points are aligned on straight line segments above or below the solid black line. The intrinsic point-to-point scatter is mostly much less than the track-to-track variations. Data in Figure 10 are from eight combined viewports of SPEX airborne. Individual viewports provide similar agreement with RSP; rms values of  $DoLP_{SPEX} - DoLP_{RSP}$  per viewport are all very similar, and there is no dependence of the agreement on viewport angle. One exception is the viewing angle  $-56^\circ$ , which has rms differences with RSP a factor of two to three larger than the mean RMS of all the viewports for all tracks. It is unclear what is the cause for a larger mismatch at the outermost viewing angle.

The agreement in radiance data in the lower two panels in Figure 9 varies from 1% to 5% rms, depending on wavelength and scene, which is considered to be excellent considering the fact that the radiometric calibration accuracy is estimated to be 4%. The adopted uncertainty for SPEX radiance measurements appears to be too conservative, and the measurements provide a better indication of the quality of radiance measurements.

At this stage, the cause(s) for the observed discrepancies in polarization measurements are under investigation and will be reported on in a future publication.



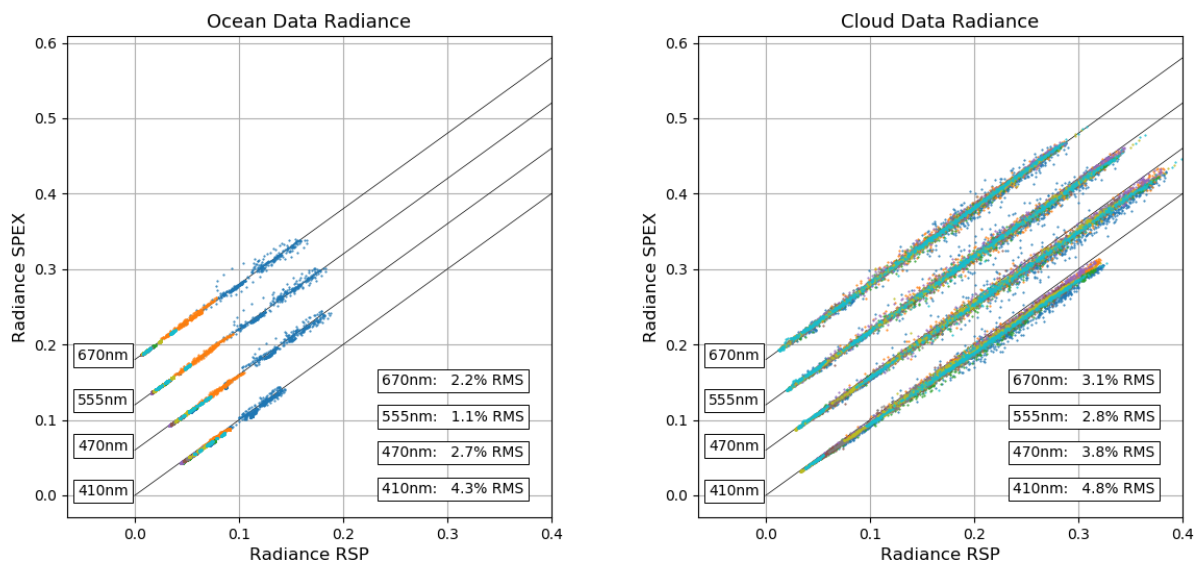


Figure 10. SPEX airborne data versus RSP data at four RSP wavelength bands centered on 410, 470, 555 and 670nm. DoLP is in dimensionless units, radiance is in units Watt/m<sup>2</sup>/nm/sterad. Top two panels are data collected over ocean and lakes, bottom two panels are from cloud scenes. Data from all viewports are combined, with different viewing angles colored separately. Data from different wavelengths are shifted vertically, with zero offset for 410nm. Solid lines represent the identity relation. For each panel, the rms difference is listed in a boxed insets. For radiance data, the rms is computed of the relative difference  $(DoLP_{SPEX} - DoLP_{RSP}) / DoLP_{RSP}$ .

## 7. CONCLUSIONS

A multi-angle spectro-polarimeter payload “SPEX airborne” has been developed for remote sensing and characterization of aerosol and cloud properties on board NASA’s atmospheric research aircraft ER-2. It employs spectral modulation to encode the state of linear polarization onto the radiance spectrum using only passive optics. Descriptions of the instrument and its subsystems are given, including operation and data processing. The polarimetric accuracy is verified to be 0.002 under lab conditions. Its radiometric accuracy is estimated to be 4%. Radiometric and polarimetric data, collected with SPEX airborne during the recent ACEPOL campaign, are compared with simultaneous observations made with RSP on the same platform, for two distinct scenes. Comparisons were made at four wavelength bands centered at 410, 470, 555 and 670nm. For clouded scenes, very good agreement is found between the two instruments at 470, 555nm and 670nm, with DoLP differences less than 0.005 rms with the DoLP reaching 60% max. For ocean scenes, including nearly 100% polarized light from the sun-glint, DoLP measurements at 555 and 470nm differ by less than 0.007. The 410nm wavelength band gives a poor match at both scenes. Radiance measurements of the two instruments are in perfect agreement with respect to the formal uncertainty of 4%. The data suggest that the radiometric accuracy of both instruments could be better than the mutual adopted estimates.

## ACKNOWLEDGEMENTS

We thank the Netherlands Space Office for the grants to develop and characterize the Optical Module “SPEX” of SPEX airborne. We thank Netherlands Organization for Scientific Research (NWO), NASA, and Hal Maring in particular, for funding the ACEPOL campaign. We thank Dave Diner for the use of calibration equipment at JPL, and thank Gerard van Harten and Brian Rheingans for assistance, support and trouble shooting during calibration measurements, calibration data processing and flight campaigns. We thank the engineering team at SRON for realizing an almost flawlessly functioning SPEX airborne system.

## REFERENCES

- [1] Hasekamp O.P., Litvinov P., Butz A., *Aerosol properties over the ocean from PARASOL multiangle photopolarimetric measurements*, J. Geophys. Res., Vol. 116, D14204, doi:10.1029/2010JD015469 (2011)
- [2] Dubovik O. et al., *Statistically optimized inversion algorithm for enhanced retrieval of aerosol properties from spectral multi-angle polarimetric satellite observations*, Atmos. Meas. Tech. 4, 975–1018 (2011)
- [3] Lacagnina et al, *Aerosol single-scattering albedo over the global oceans: Comparing PARASOL retrievals with AERONET, OMI, and AeroCom models estimates*, J. Geophys. Res. Atmos., 120, 9814–9836, doi:10.1002/2015JD023501 (2015)
- [4] Lacagnina C., Hasekamp O.P., Torres, O., *Direct radiative effect of aerosols based on PARASOL and OMI satellite observations*, J. Geophys. Res. Atmos., 122, doi:10.1002/2016JD025706 (2017)
- [5] Russel et al. *A multiparameter aerosol classification method and its application to retrievals from spaceborne polarimetry*, J. Geophys. Res. Atmos., 119, 98389863, doi:10.1002/2013JD021411 (2014)
- [6] Deschamps, P. Y., F. M. Bréon, M. Leroy, A. Podaire, A. Bricaud, J. C. Buriez, and G. Sèze (1994), The POLDER mission: Instrument characteristics and scientific objectives, IEEE Trans. Geosci. Remote Sens., 32, 598–615.
- [7] Cairns, B., Russell, E.E., Travis, L.D., *Research scanning polarimeter: calibration and ground-based measurements*. In: Goldstein, D.H., Chenault, D.B. (Eds.), Polarization: Measurement, Analysis, and Remote Sensing. vol. 3754. pp. 186–197 of Proc. SPIE (1999).
- [8] Cairns B., Russell E.E., LaVeigne J., Tennant P.M.W., *Research scanning polarimeter and airborne usage for remote sensing of aerosols*, Proceedings of SPIE Vol. 5158 (2003)
- [9] Peralta, R.J., Nardell, C., Cairns B., Russell E.E., Travis L.D., Mishchenko M.I., Fafaul B. A., and Hooker R. J., *Aerosol polarimetry sensor for the glory mission*, Proc. SPIE 6786, 67865L (2007)
- [10] Mishchenko, M.I., 2006. Glory. In: Parkinson, C.L., Ward, A., King, M.D. (Eds.), Earth Science Reference Handbook: A Guide to NASA's Earth Science Program and Earth Observing Satellite Missions. National Aeronautics and Space Administration, pp. 141–147.
- [11] Mishchenko, M.I., Cairns, B., Kopp, G., Schueler, C.F., Fafaul, B.A., Hansen, J.E., Hooker, R.J., Itchkawich, T., Maring, H.B., Travis, L.D., 2007. *Accurate monitoring of terrestrial aerosols and total solar irradiance: introducing the Glory mission*. Bull. Am. Meteorol. Soc. 88, 677–691.
- [12] Diner D.J. et al, *The Airborne Multiangle SpectroPolarimetric Imager (AirMSPI): a new tool for aerosol and cloud remote sensing*, Atmos. Meas. Tech. 6, 2007–2025 (2013).
- [13] Diner D.J. et al. , *First results from a dual photoelastic- modulator-based polarimetric camera*, Appl. Opt. 49, 2929- 2946 (2010)
- [14] Van Harten, G. et al. , *Calibration and validation of Airborne Multiangle SpectroPolarimetric Imager (AirMSPI) polarization measurements*, Applied Optics, Vol 57, No17 (2018)
- [15] J. V. Martins, *Measurements of polarized light scattering by atmospheric particles with the passive aerosol and cloud suite (PACS) in Presentation*. Electromagnetic and Light Scattering XIV (2013).
- [16] Martins J.V., *HARP: hyper-angular rainbow polarimeter CubeSat*, in Presentation. ESTO Science and Technology Forum (2016).
- [17] Erik Laan, Daphne Stam, Frans Snik, Theodora Karalidi, Christoph Keller, Rik ter Horst, Ramon Navarro, Gijsbert Oomen, Johan de Vries, Ruud Hoogeveen, "The Spectropolarimeter for Planetary Exploration: SPEX", Proc. SPIE 10566, International Conference on Space Optics - ICSO 2008, doi: 10.1117/12.2308240 (2008)
- [18] Rietjens J.H.H. et al., *SPEX: The Spectropolarimeter for Planetary Exploration*, Proc. of the ICSO 2010, (2010)
- [19] Snik, F., Rietjens, J. H. H., van Harten, G., Stam, D. M., Keller, C. U., Smit, J. M., Laan, E. C., Verlaan, A. L., ter Horst, R., Navarra, R., Wielinga, K., Moon, S. G. and Voors, R., "SPEX: The Spectropolarimeter for Planetary Exploration", Proc. SPIE 7731, 77311B (2010)
- [20] Van Harten, G. et al., *Prototyping for the Spectropolarimeter for Planetary EXploration (SPEX): calibration and sky measurements*, Proceedings of SPIE 2011, Vol 8160 (2011)

- [21] Rietjens, et al., J.H.H.H et al., *SPEX: a highly accurate spectropolarimeter for atmospheric aerosol characterization*, Proceedings of ICSO (2014).
- [22] Van Harten, G., *Spectropolarimetry for Planetary Exploration*, Ph.D. Thesis (2014)
- [23] Rietjens J.H.H.R., *Accurate spectrally modulating polarimeters for atmospheric aerosol characterization*, *Proceedings of SPIE*, Volume 9613, (2015)
- [24] Van Amerongen, A.H., et al, *SPEX, the Dutch roadmap towards aerosol measurement from Space*, Proceedings ICSO (2016).
- [25] Van Amerongen, A.H., et al, *SPEXone: A compact multi-angle spectro-polarimeter*, Proceedings ICSO (2018).
- [26] Snik F., Karalidi, T., Keller, C. U., *Spectral modulation for full linear spectroscopy*, *Applied Optics* 48, 1337 (2009)
- [27] Snik F. et al, *SPEX: An in-orbit spectropolarimeter for planetary exploration*, Proceedings of SPIE 2008, Vol. 7010 (2008)
- [28] Van Harten, G. et al, *Atmospheric aerosol characterization with a ground-based SPEX spectropolarimetric instrument*, *Atmos. Meas. Tech. Discuss.*, 7, 5741–5768, (2014)
- [29] Müller, D. et al, *Airborne Multiwavelength High Spectral Resolution Lidar (HSRL-2) observations during TCAP 2012: vertical profiles of optical and microphysical properties of a smoke/urban haze plume over the northeastern coast of the US*, *Atmos. Meas. Tech.*, 7, 3487–3496, 2014
- [30] McGill M., et al, *Cloud Physics Lidar: instrument description and initial measurement results*, *Appl. Opt.* 41, 3725-3734 (2002)
- [31] Jarvis A, Reuter H.I., Nelson A., and E. Guevara (2008). Hole-filled seamless SRTM data V4, International Centre for Tropical Agriculture (CIAT), available from <http://srtm.csi.cgiar.org>, J.
- [32] Smit, J.M. et al., *SPEX airborne spectro-polarimeter calibration and performance*, to be submitted to *Applied Optics*